Presented at the 37th European PV Solar Energy Conference and Exhibition, 7-11 September 2020

EARLY STAGE QUALITY ASSESSMENT IN SILICON INGOTS FROM MDP BRICK CHARACTERIZATION

A.S. Kovvali[1], M. Demant[1], B. Rebba[1], N. Schüler[2], J. Haunschild[1], S. Rein[1]

[1] Fraunhofer Institute for Solar Energy Systems, Heidenhofstrasse 2, 79110 Freiburg, Germany
[2] Freiberg Instruments GmbH, Delfter Str. 6, D-09599 Freiberg

ABSTRACT: Feedback on the material quality of silicon ingots is highly beneficial in the photovoltaic production chain. It is crucial for crystal growers to improve the quality and optimize the crystallization process. Moreover, for solar cell manufacturers, knowing the quality beforehand helps to sort out the bad quality material thereby reducing the costs and enhancing the total yield. Therefore, rating material quality already on the brick level is highly valuable for the effective optimization of the value chain in both directions. In this paper, we propose a method to classify the silicon bricks based on their electrical quality. Due to our comprehensive data set and feature detection, the model is capable to predict the quality of even edge and corner bricks of the ingot. We introduce a novel feature extraction method to quantify quality-related features from spatially-resolved microwave-detected photoconductivity (MDP) brick measurements. Further, a machine-learning-based prediction model is developed to predict the open-circuit voltage (V_{oc}) of solar cells from these features. A comparative analysis for brick quality estimation for inner and outer bricks of high-performance multi (HPM) and cast-mono (CM) silicon bricks is provided. The best mean absolute error in prediction achieved for HPM and CM materials is 3.1 mV and 4.8 mV, respectively.

Keywords: Ingot quality, material characterization, cast-mono Silicon, high-performance multicrystalline Silicon, MDP, brick rating

1 INTRODUCTION

Early stage material quality assessment is required for crystal growers for the development of new material classes like smart mono [1]. For cell manufacturers, determining the material quality helps in proper material selection for cost-effective solar cell production. Crystal growers have put continuous effort into the enhancement of electrical quality in silicon ingots. This has led to the improvement of silicon material quality during crystallization and thereby the overall solar cell performance. Industrialization and further optimization of new crystallization techniques, like smart mono, require rapid assessment of silicon ingot quality.

In silicon solar cells, the cost of the raw silicon wafers dominates the total cost of the finished solar cell [2]. Therefore, for the solar cell manufacturers, it is important to know the quality of the wafers beforehand to discard wafers from low quality parts of the bricks early in the production chain.

Traditionally in a photovoltaic production chain, feedback to the crystal growers is provided based on the quality of final solar cell efficiencies. With the help of wafer rating models, early prediction of the quality is possible [3, 4]. However, dicing the bricks into wafers, wafer tracking, and data handling requires additional effort, time and expenses. This results in long feedback times and complicated feedback loops and thus reduces the possible speed of process optimization in crystal growth. Thus, such a brick rating model is advantageous over a classical wafer rating model.

Using the MDP technique for brick characterization, it is possible to measure the spatially-resolved carrier lifetime and resistivity maps of silicon bricks [5]. MDP lifetime measurements are contactless and inline feasible and do not require further calibration [6]. The bulk lifetime of the material has a significant influence on the final solar cell efficiency [7]. As bricks represent semi-infinite samples with only one surface, lifetime measurements on brick level are much less affected by surface recombination than lifetime measurements on the as-cut wafer stage [8]. Thus, lifetime measurements on brick level allow insight into the actual bulk lifetime of the material, which is not possible on as-cut wafer level. . Therefore, it is possible to estimate the maximum reachable efficiency of the material from the carrier lifetimes measured on brick level.

Earlier, a similar brick rating technique using photoluminescence imaging (PL) of the bricks to predict the open-circuit voltage of passivated emitter and rear cells (PERC) has been proposed in Ref. [9]. Here. the harmonic mean of carrier lifetime from brick measurements and the dislocations from as-cut wafer measurements are used to predict a product of short circuit current (J_{sc}) and V_{oc} for inner bricks only. In our study, MDP lifetime measurements are used for the first time as basis for a brick rating model. Moreover, both, lifetime and dislocations are extracted from brick measurements only. Further, we extend this approach to outer bricks, which brings new challenges, as the defect distribution of the brick measurements does not directly reflect the defect distribution in the inner parts of the wafer. Therefore, we propose a new estimation of lifetime by weighing the harmonic mean from different sides of the outer bricks. Special care was taken during feature extraction for the outer bricks which are in contact with the crucible walls.

Overall, the work presents a brick rating model to predict the performance of solar cells from brick characterization only. Such a brick rating model enables a simple and early stage comparison between multiple crystallization cycles in terms of their electrical quality for both, HPM and cast-mono silicon.

2 APPROACH

Our approach combines a relevant data description of the material according to known physical relations and a subsequent empirical data model. An overview of our three-step approach is shown in the Figure 1. First, using MDP technique, we measure spatial lifetime and resistivity images from four sides of the brick. Second, from the measured brick images, we extract physically related features using traditional image processing techniques, deep learning network and assign these features to individual ingot heights and wafers respectively. Third, a machine learning prediction model is trained to learn predicting V_{oc} of the solar cells from the extracted brick features virtually assigned to the individual wafers. Each of the steps is described in detail in following Sections.

Figure 1: Overview of approach for brick rating model

2.1 Brick characterization

For each of the brick, the MDP maps for lifetime and resistivity are measured with a resolution of 1 mm on all 4 brick sides (east, north, west and south). While resistivity is measured inductively, lifetime is measured by means of the MDP technique using a 900 nm laser for excitation with a penetration depth of 500 µm and duration of excitation pulse of 1000 µs. MDP lifetime and resistivity measurements of an edge brick from all four sides are shown in Figure 2 and Figure 3. The lifetime distribution of our measured bricks is between 10 µs and 82 µs. The resistivity of the material varies between 1-3 Ω/cm^2.

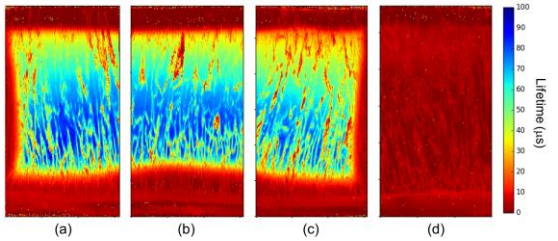

Figure 2: Lifetime measurement (a) east (b) north (c) west and (d) south sides of the brick

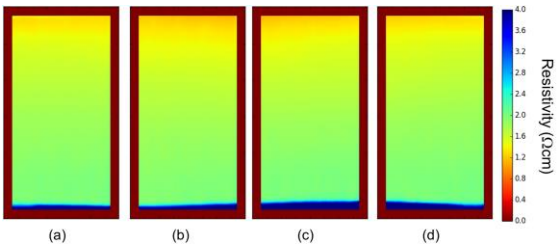

Figure 3: Resistivity measurement (a) east (b) north (c) west and (d) south sides of the brick

The measured bricks are wafered and these as-cut wafers are processed to solar cells. Each of the solar cells is then associated to the respective pixels rows at the corresponding ingot height in the MDP brick measurements. Detail description of data assignment between brick and solar cell is explained in Section 2.4.

2.2 Feature extraction

For each of the brick, we extract the following physically related features listed below,

a) Contaminated side regions
b) Contamaninated top and bottom regions
c) Lifetime
d) Resistivity
e) Dislocations

(a) *Contaminated side regions:* for the bricks in contact with the crucible walls, the impurities diffuse into the material from brick sides. These regions negatively impact the performance of the solar cell and are only partially gettered during the cell process [10, 11]. These regions have low lifetime values as visible in MDP lifetime measurements. Due to their positioning on the brick sides, it is possible to distinguish from other defects. In Figure 2 (a) and (c), the low lifetime values along the vertical edges correspond to contaminated regions. From these images, the area fraction of contaminated regions (A_{cont}) is extracted as a feature using image processing techniques. The calculated A_{cont} is normalized between the range of values 0 and 1.

(b) *Contaminated bottom or top regions:* the bottom and top parts of the bricks have lower lifetime values due to in-diffusion of impurities from the crucible bottom, and segregation and back-diffusion of impurities during crystallization in the brick top. These regions have a different gettering behavior as compared to contaminated regions [12]. Therefore, we classify these regions as contaminated bottom and top regions during feature extraction.

The Figure 4 shows an example of extracted contamination regions on the sides, marked in yellow color and contaminated regions at top and bottom marked in orange color.

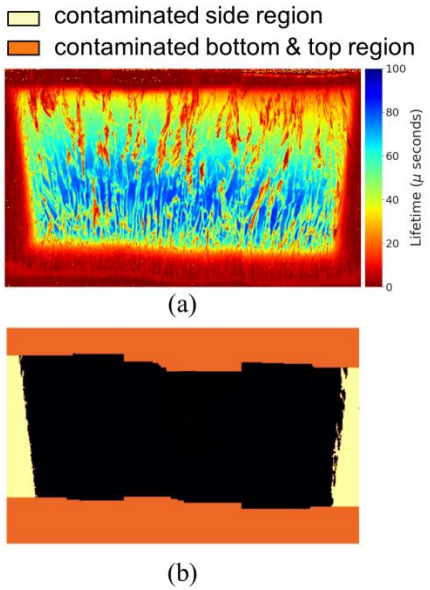

Figure 4: Lifetime images from east, north and west sides of an edge brick stitched together and (b) extracted contaminated side, bottom and top regions

(c) *Lifetime:* the lifetime of the material is directly proportional to the final performance of the solar cell. For inhomogeneous lifetime distributions, it is known from literature that the harmonic mean of lifetime τ_{HM} corresponds best to open circuit voltage [13]. Therefore we extract the harmonic mean of the individual wafer sample from four sides of the brick measurements according to equation **Error! Reference source not found.**.

$$T_{HM} = \frac{1}{n} * \sum_{i=1}^{n} (\tau_i^{-1}) \qquad (1)$$

where τ_i is the lifetime of an individual pixel and n is the total number of pixels in the pixel row from four sides of MDP lifetime image.

However, in case of the edge and corner bricks of the ingot, the lifetime images of the brick sides, which are in contact with crucible walls, have low lifetime values. Such a lifetime image of an edge brick is shown in Figure 2 (d). According to equation **Error! Reference source not found.**, each side of the brick contributes 25% to the total harmonic mean. This leads to underestimation of harmonic mean since the area of contamination can also be less than 25%. Therefore, we propose a weighted harmonic mean by (i) identifying regions of reduced lifetime due to crucible sides as contaminations and (ii) estimating the area of these contaminated regions A_{con} in the inner regions of the wafer. The proposed rating model uses the (iii) area weighted harmonic mean, which is given according to equation **Error! Reference source not found.**.

$$T_{WHM} = (1 - \frac{A_{con}}{A}) * \frac{1}{|\bar{c}|} \sum_{i \in \bar{c}} \tau_i + (\frac{A_{con}}{A}) * \frac{1}{|c|} \sum_{i \in c} \tau_i \qquad \mathbf{(2)}$$

where, A is the total area of the sample, i is individual pixel and c is the set of indices of the measured MDP signal in contaminated region and $\bar{c}$ in non-contaminated regions.

(d) *Resistivity:* the resistivity of the material is influenced by the doping concentration. The base resistivity of the material influences the final performance of the solar cell depending on the cell type [14]. Therefore, from the MDP resistivity images, the average resistance of the wafer is calculated.

(e) *Dislocations:* structural defects like dislocations have adverse effects on final performance of the solar cells [15]. Since the resolution of the brick lifetime images is low, it is difficult to extract dislocations using traditional image processing techniques. Therefore, we trained a deep learning network U-Net, to detect dislocations from MDP lifetime images [16].

For training the U-Net, we hand labelled MDP lifetime images from 25 bricks. The dislocation pixels in the images are manually labelled and pairs of lifetime images and labels are used for training. The network is trained patch wise by cropping the input images randomly to a size of 128 x 128 pixels. We then trained the network for 120k iterations and optimize using L2 loss as in [17] . The network trained can predict the dislocations from lifetime images of 128 x 128 pixels. Since the MDP lifetime images of the complete brick are larger than 128 pixels, patch wise detections are stitched together into the complete lifetime MDP image.

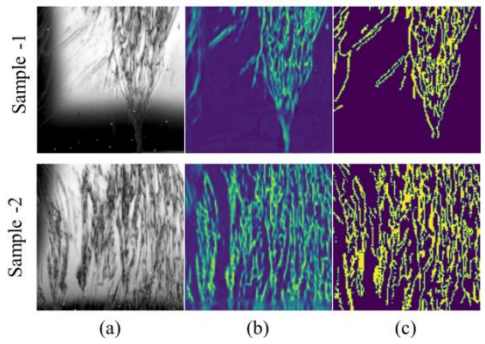

Figure 5: Dislocation detection from two samples. (a) Cropped lifetime image (b) detected dislocations and (c) hand labelled image.

The Figure 5 shows dislocation detection from MDP lifetime images of two bricks cropped at different regions. The dislocation detection is robust also in contrast invariant regions as shown above.

2.3. Brick rating

For the description of each brick segment, extracted features and V_{oc} values of the solar cells constitute inputs for training a nonlinear random forest (RF) based regression model [18] .

However, random forest based regression is limited to the boundaries of the training dataset predictor values and it is not possible for extrapolation in prediction [19]. Therefore, we use a hybrid of linear regression and nonlinear RF regression models called "Regression Enhanced Random Forests" (RERF) as in [20].

In the first step for RERF, a multivariate regression model is applied without any regularization. The residuals from the regression are calculated for the training dataset. Then a RF model is trained on the residuals calculated previously for the same input feature vector. The final prediction response of RERF for given predictor value is given by

$$\widehat{Y}(X_0) = \underbrace{X_0\widehat{\beta}_\lambda}_{\text{Multi variate regression}} + \underbrace{T_{m,s}(X_0)}_{\text{Random forests}}$$

where $\hat{Y}$ is the final prediction, X_0 is the input feature vector, $\hat{\beta}$ are the weights of regression model and λ, m, s are hyper parameters.

The values for the hyper parameters λ, m, s are 0.5, 0.33 and 5, respectively, according to [21].

2.4. Exploratory data preparation

Missing data: due to the presence of dirt and surface irregularities, the signal to noise ratio of the sensor in MDP measurement is low. The lifetime in these spots cannot be measured and thus a 'nan' value is generated. These missing values are detrimental during feature extraction. Therefore, we interpolate the missing values

using the nearest-neighbor values with a grid structure of 3x3 pixels.

Data association: we assign each of the pixel rows in these images to 1 silicon wafer or solar cell. For example, the i^{th} pixel row from all the four sides of the measurement corresponds to a solar cell / wafer at brick height of i mm. However, adding the kerf loss of 200-300 µm each wafer of 200 µm thickness corresponds to ~500 µm in brick height, i.e. ~ 2 wafers originate from 1 mm brick length. We assume that the defect distribution and material quality does not differ much between two neighboring wafers. To increase the assignment tolerance between brick and wafer data, we thus associate 1 wafer/cell to 1 mm thickness in the brick measurements.

3 Experimental

3.1 Experimental data

Within our experiment, a comprehensive data set was created for model development and evaluation. Our data set consists of around 1200 industrial Al-BSF solar cells from 19 bricks of HPM and CM from different brick positions. Bricks from two different crucible sizes G2 and G6 with ingot heights of 200-220 mm for G2 and 300-320 mm for G6 are present in our dataset.

The entire dataset is broadly classified into 4 different classes. 19 bricks are divided into two groups HPM all bricks and CM depending on the material type i.e. HPM and CM silicon. The bricks from HPM material are further divided into subgroups HPM inner and HPM outer based on their position in ingot. The CM bricks in our dataset consist of only 1 inner brick and therefore the group is not further subdivided. These different material classes along with number of bricks are shown in Table I.

In total, 926 solar cells from HPM material and 235 solar cells from CM material are considered. Solar cells whose wafer samples have low lifetime values from measured MDP signal are discarded and only the samples with weighted harmonic mean of at least 7 µs are considered in our experiment.

Table I: Dataset, number of bricks/cells of different material types

	HPM all	HPM inner	HPM outer	CM
G2/G6 bricks	12	6	6	7
Solar cells	926	475	451	235
G2 bricks	3	3	-	5
G6 bricks	9	3	6	2

3.2 Model evaluation

For each of the classes, a separate prediction model is developed and tuning parameters are optimized. During training, each brick in the grouped dataset is selected once as test brick and the model is trained on the remaining bricks. Thus, we realized a complete blind test, since the data from the test brick are not included in the training. The prediction accuracy of the model is calculated by averaging test brick errors over all the bricks in the group.

3.3 Experimental evaluations

In our work, we conduct 4 different evaluations on our data using the developed brick rating model.

i. In our first evaluation the model quality for different material classes is investigated. For each material class in Section 3.1, we train a separate prediction model as described in 3.2. During feature extraction, we extract the area fraction of contaminated sides, bottom and top regions, weighted harmonic mean of lifetime, the area fraction of dislocations and average resistivity as explained in Section 2.2.
ii. We investigate the impact of the weighted harmonic mean as quality parameter on the prediction accuracy. We replace the weighted harmonic mean with standard harmonic mean and repeat the evaluation for all of the material classes. Further, we compare the prediction results of standard harmonic mean with weighted harmonic mean of lifetime.
iii. We analyze the applicability of our model for quality inspection by sorting bricks based on the predicted results. We further determine the brick quality of individual bricks. Four bricks with different material quality are selected and their quality is determined using the proposed brick rating model.
iv. Detailed analysis on prediction accuracy for the samples over brick height is carried out. Two central bricks from HPM with their measured and predicted V_{oc} values over the brick height are compared.

3.4 Experimental results

From our evaluations in Section 3.3, we derive following results.

Figure 6 shows the prediction accuracy of the proposed model from evaluations (i) in Section 3.3. The proposed brick rating model predicts the solar cell V_{oc} with reasonable accuracy for inner and outer HPM bricks as seen in Figure 6. For the CM bricks, the prediction accuracy is lower than for HPM bricks.

Figure 6 also shows a comparison of the results using a prediction model with weighted harmonic mean and harmonic according, respectively, according to evaluation (ii) in Section 3.3. For all the material classes, the model with weighted harmonic mean has lower mean absolute errors (MAE) in prediction.

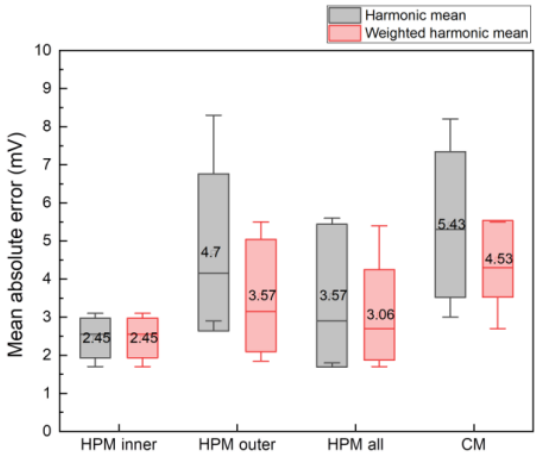

Figure 6: Prediction quality for HPM and CM bricks from inner, outer positions in ingot.

Quality predictions for four bricks as described in evaluation (iii) in Section 3.3 are shown in Figure 7. Brick 1 and 2 have lower quality (~ 4 mV) compared to brick 3 and 4. The predicted V_{oc} distribution of these bricks is comparable to measured V_{oc} distribution with

low errors. This shows the ability of the proposed brick rating model to distinguish bad quality bricks.

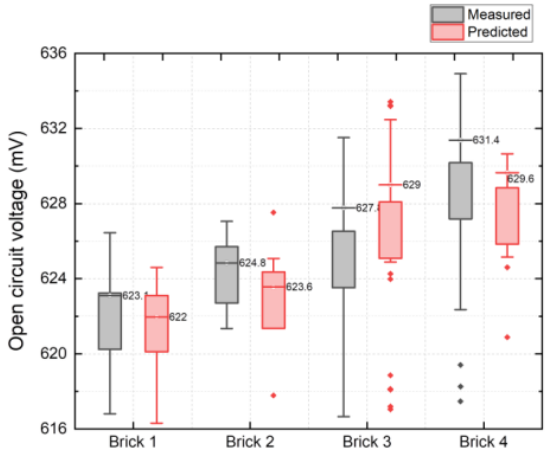

Figure 7: Measured and predicted V_{oc} distribution of four bricks with different material quality.

In our detailed analysis from evaluation (iv) in Section 3.3, predicted and measured V_{oc} for two central bricks with MAE of 2.8 mV and 1.8 mV respectively are shown as a function of brick height in the Figure 8. The predicted V_{oc} for the brick 2 follows the measured V_{oc} even at the strong slopes in the bottom and top regions below 60 mm and above 175 mm brick height. For brick 1, the model slightly overestimates the V_{oc} towards the top of the brick leading to slight errors in prediction.

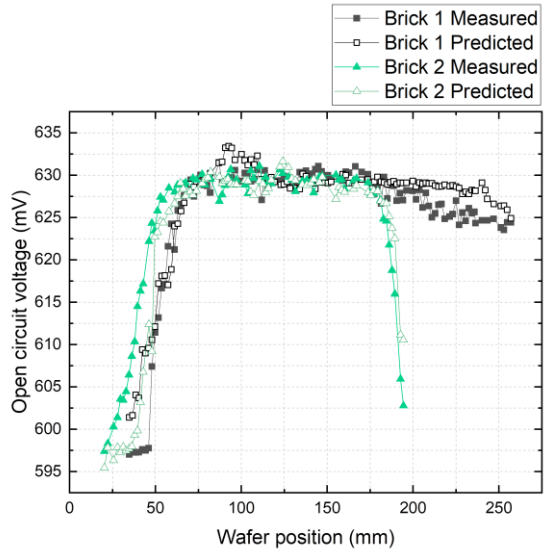

Figure 8: Comparison of measured (closed symbols) and predicted (open symbols) V_{oc} values as function of brick height for two central bricks from different ingots.

4 DISCUSSION

From our evaluations and results (i), (ii) and (iii) in Section 3.3 and 3.4, we have shown that the proposed brick rating model can predict the quality of the bricks for different material classes. It is also possible to distinguish low and high quality bricks using the proposed brick rating model.

From our detailed hight-dependent evaluation (iv) in Section 3.3, we observe two scenarios leading to larger errors in prediction. First, for brick 1, a small bump in the predicted V_{oc} curve is observed in the region of 80-100 mm brick height. The predicted V_{oc} is higher than the measured values as seen in the Figure 8. Even though the lifetime in this region is higher, the measured V_{oc} remains low which may be caused by structure-dependent efficiency limitations due to the Al-BSF cell process applied here [22]. Thus, the wafers with higher lifetime values lead to errors in prediction.

Secondly, for the same brick 1, large errors are also observed in the region higher than 200 mm in the brick. The predicted V_{oc} values in these regions are overestimated compared to the measured ones. This is because the dislocations determined at the brick surface do not represent the true dislocation distribution over the entire sample area. **Error! Reference source not found.** (a) shows a PL image of one of the wafer in this region.

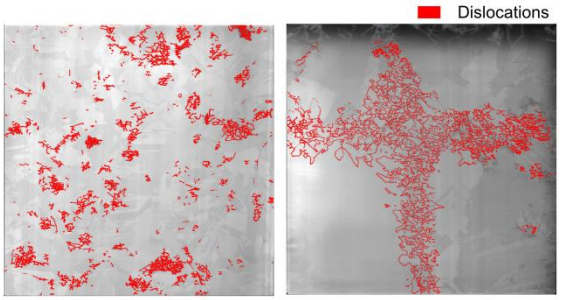

Figure 9: PL image of a wafer from a (a) HPM brick (Brick 1) at a height of 225 mm and (B) CM brick at a height of 124 mm.

Most of the dislocation clusters appear in the inside part of the wafers which are not visible within the brick measurements.

The proposed brick rating model allows accurate prediction for homogeneous materials but has limited accuracy in materials with inhomogeneous defect distributions within outer and inner parts of the brick. The higher prediction error for cast-mono material result due to errors in estimation of dislocation structures from brick measurements to true density of dislocations. During cast-mono crystallization functional defects such as grain boundaries are introduced to control the ingrowth of parasitic grains and dislocation clusters. In these bricks, the dislocations arise close to the grain boundaries and grow further into the material as seen in **Error! Reference source not found.** (b). Therefore, it is challenging to estimate the actual defect distribution for such bricks only from MDP brick lifetime images.

Finally, Figure 10 motivates the reason for restricting wafer samples with at least 7 µs of carrier lifetime during training and evaluation of prediction model. The Figure 10 (a) shows the average lifetime (red), weighted harmonic mean (blue) and measured V_{oc} (green) over the brick height. Figure 10 (b) shows the four sides of MDP lifetime image.

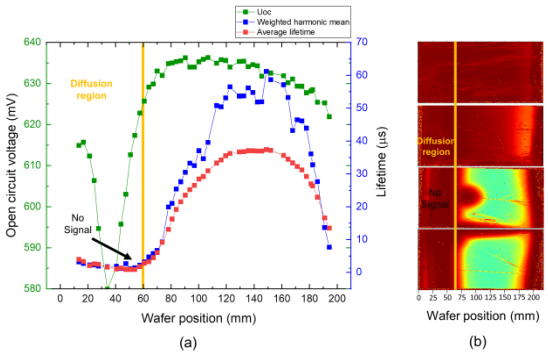

Figure 10: Analysis of contaminated bottom and top regions in a cast-mono brick.

In the region below 60 mm brick height, it is not possible to extract any features due to low lifetime values. These low lifetime values occur due to the in-diffusion of impurities into the brick from the crucible bottom. However, during the solar cell process, impurities in these regions are gettered effectively. Therefore, we see a rise in measured V_{oc} for the solar cells even with low lifetime values in diffusion regions. Since we cannot observe distinguishing features in the diffusion regions which explain the strong variations in V_{oc}, only wafer samples with their harmonic mean higher than 7 µs are considered in the above evaluation.
The gettering effect of the specific solar cell process, which improves the lifetime, can be seen only after the process itself. Appropriate rating for these special wafers will be addressed in future developments.

5 CONCLUSION

We introduce a method for quantifying material quality based on the brick measurements only. We show a comparative analysis of the brick rating method on bricks from both inner and outer positions in the ingot. The proposed rating model successfully predicts the quality of HPM and CM bricks with MAE of 3.06 mV and 4.85 mV, respectively.

Further, we quantify structural defects in MDP lifetime brick measurements for both HPM and CM materials. We suggest calculating a weighted harmonic mean of lifetime for outer bricks and compare its performance over standard harmonic mean.

From the prediction results, we observe that a simple non-linear regression model like RERF is sufficient for predicting Al-BSF processed solar cells from HPM material with reasonable errors. This is due to the fact that cell efficiency is limited in the high-lifetime regions by the cell process and not by material quality. This however changes in the case of a PERC process which is more sensitive to material quality due to its higher efficiency potential which will be further investigated. Moreover, applicability of the brick rating model to materials with less structural defects seems interesting.

6 ACKNOWLEDGEMENT

The work has been financed by the German Ministy for Ecomomic Affairs and Energy (BMWi) within the frame of the project Q-Crystal (contract number 0324103A-G). The authors gratefully acknowledge sample preparation along the value chain by ALD, Logomatic and PV-Crystalox.

7 REFERENCES

References

[1] S. Riepe, P. Krenckel, Y. Hayama, A. Hess, T. Troetschler, K. Kutsukake, Stéphan, Maus, F. Schindler, and N. Usami, “ENHANCED MATERIAL QUALITY IN SMART MONO-SI BLOCK CAST INGOTS BY INTRODUCTION OF FUNCTIONAL DEFECTS,” in 2019.

[2] A. Louwen, W. van Sark, R. Schropp, and A. Faaij, “A cost roadmap for silicon heterojunction solar cells,” *Solar Energy Materials and Solar Cells*, vol. 147, pp. 295–314, http://www.sciencedirect.com/science/article/pii/S0927024815006741, 2016.

[3] J. Haunschild, M. Glatthaar, M. Demant, J. Nievendick, M. Motzko, S. Rein, and E. R. Weber, “Quality control of as-cut multicrystalline silicon wafers using photoluminescence imaging for solar cell production,” *Solar Energy Materials and Solar Cells*, vol. 94, no. 12, pp. 2007–2012, 2010.

[4] M. Demant, P. Virtue, A. Kovvali, S. X. Yu, and S. Rein, “Learning Quality Rating of As-Cut mc-Si Wafers via Convolutional Regression Networks,” *IEEE J. Photovoltaics*, vol. 9, no. 4, pp. 1064–1072, 2019.

[5] N. Schuler, D. Mittelstrass, K. Dornich, J. R. Niklas, and H. Neuhaus, “Next generation inline minority carrier lifetime metrology on multicrystalline silicon bricks for PV,” in *2010 35th IEEE Photovoltaic Specialists Conference*, Honolulu, HI, USA, Jun. 2010 - Jun. 2010, pp. 852–857.

[6] N. Schüler, B. Berger, A. Blum, K. Dornich, and J. R. Niklas, “High Resolution inline Topography of Iron in p-Doped Multicrystalline Bricks by MDP,” *Energy Procedia*, vol. 38, pp. 176–182, http://www.sciencedirect.com/science/article/pii/S1876610213013519, 2013.

[7] S. Wasmer, J. Greulich, H. Höffler, N. Wohrle, M. Demant, F. Fertig, and S. Rein, “Impact of Material and Process Variations on the Distribution of Multicrystalline Silicon PERC Cell Efficiencies,” *IEEE J. Photovoltaics*, vol. PP, pp. 1–11, 2016.

[8] R. Krain, R. Falster, and R. Sinton, “Determination of the Bulk Lifetime of Bare Multicrystalline Silicon Wafers,” *Prog. Photovolt: Res. Appl.*, vol. 18, pp. 204–208, 2010.

[9] B. Mitchell, D. Chung, Q. He, H. Zhang, Z. Xiong, P. P. Altermatt, P. Geelan-Small, and T. Trupke, “PERC Solar Cell Performance Predictions From Multicrystalline Silicon Ingot Metrology Data,” *IEEE J. Photovoltaics*, vol. 7, no. 6, pp. 1619–1626, 2017.

[10] M. C. Schubert, J. Schon, F. Schindler, W. Kwapil, A. Abdollahinia, B. Michl, S. Riepe, C. Schmid, M. Schumann, S. Meyer, and W. Warta, “Impact of

Impurities From Crucible and Coating on mc-Silicon Quality—the Example of Iron and Cobalt," *IEEE J. Photovoltaics*, vol. 3, no. 4, pp. 1250–1258, 2013.

[11] F. Sturm, M. Trempa, S. Schwanke, K. Schuck, C. Kranert, C. Reimann, and J. Friedrich, "Solid state diffusion of metallic impurities from crucible and coating materials into crystalline silicon ingots for PV application," *Journal of Crystal Growth*, vol. 540, p. 125636, http://www.sciencedirect.com/science/article/pii/S0022024820301597, 2020.

[12] T. Eguchi, T. Hirasawa, I. Yamaga, M. Dhamrin, T. Saitoh, and K. Kamisako, "Effect of Directional Solidification Processes on Diffusion Length Distribution of High Quality Multicrystalline Silicon Ingots," in 2005.

[13] H. Wagner, M. Müller, G. Fischer, and P. P. Altermatt, "A simple criterion for predicting multicrystalline Si solar cell performance from lifetime images of wafers prior to cell production," *Journal of Applied Physics*, vol. 114, no. 5, p. 54501, 2013.

[14] H. Steinkemper, M. Hermle, and S. W. Glunz, "Comprehensive simulation study of industrially relevant silicon solar cell architectures for an optimal material parameter choice," *Prog. Photovolt: Res. Appl.*, vol. 24, no. 10, pp. 1319–1331, 2016.

[15] A. Kovvali, M. Demant, T. Trötschler, J. Haunschild, and S. Rein, "About the relevance of defect features in as-cut multicrystalline silicon wafers on solar cell performance," in Lausanne, Switzerland, 2018, p. 130011.

[16] O. Ronneberger, P. Fischer, and T. Brox, "U-Net: Convolutional Networks for Biomedical Image Segmentation," in *Medical Image Computing and Computer-Assisted Intervention - MICCAI 2015*, 2015, pp. 234–241.

[17] K. Janocha and W. M. Czarnecki, "On Loss Functions for Deep Neural Networks in Classification," *CoRR*, vol. abs/1702.05659, 2017.

[18] A. Liaw and M. Wiener, "Classification and Regression by randomForest," *R News*, vol. 2, no. 3, pp. 18–22, https://CRAN.R-project.org/doc/Rnews/, 2002.

[19] C. Tang, D. Garreau, and U. von Luxburg, "When do random forests fail?," in *Advances in Neural Information Processing Systems 31*, S. Bengio, H. Wallach, H. Larochelle, K. Grauman, N. Cesa-Bianchi, and R. Garnett, Eds.: Curran Associates, Inc, 2018, pp. 2983–2993.

[20] H. Zhang, D. Nettleton, and Z. Zhu, *Regression-Enhanced Random Forests*.

[21] S. Bernard, L. Heutte, and S. Adam, "Influence of Hyperparameters on Random Forest Accuracy," in 2009.

[22] S.W. Glunz, R. Preu, and D. Biro, "1.16 - Crystalline Silicon Solar Cells: State-of-the-Art and Future Developments," in *Comprehensive Renewable Energy*, Ali Sayigh, Ed., Oxford: Elsevier, 2012, pp. 353–387.